Available online at www.sciencedirect.com
SCIENCE DIRECT®
Journal of Power Sources 131 (2004) 270–277
JOURNAL OF POWER SOURCES
www.elsevier.com/locate/jpowsour

Relationship between electrochemical properties of SOFC cathode and composition of oxide layer formed on metallic interconnects

K. Fujita [a,*], T. Hashimoto [b], K. Ogasawara [a], H. Kameda [a], Y. Matsuzaki [a], T. Sakurai [a]

[a] *Technical Research Institute, Tokyo Gas Co. Ltd., 16-25, Shibaura, 1-chome, Minato-ku, Tokyo 105-0023, Japan*
[b] *Department of Applied Physics, College of Humanities and Sciences, Nihon University, Nihon, Japan*

Received 3 October 2003; accepted 16 December 2003

Abstract

A Cr-poisoning of SOFC cathode was studied using half-cells with alloy separators of various Cr-content. The surfaces of the oxide layer formed on the alloys were observed using energy dispersion X-ray analysis, and the precipitation of Cr at the interface between YSZ electrolyte and the cathode was studied using electron probe micro analysis. All the Cr-containing alloys were found to promote cathode degradation. However, the time dependencies of overvoltage in half-cell tests were different from one another in three kinds of alloy materials. We found that the reason of the difference was in relation to the Cr_2O_3 and the $MnCr_2O_4$ in the oxide layer formed on the alloy surface. Tests of single-cell stacks were also performed with these alloy separators. The degradation of stack voltage was large for all the stacks, and that was consistent with the half-cell tests. The reason for the large degradation was found to be a formation of $SrCrO_4$, which was presumably synthesized by the reaction of Cr_2O_3 in the oxide layer on the alloy and Sr diffused from the cathode. Therefore, it is necessary to develop a component in which the alloy does not contact the cathode directly.

Keywords: Solid oxide fuel cell; Cr-poisoning; Metallic interconnect; Half-cell

1. Introduction

The use of alloy materials for SOFC interconnects has some advantages, such as reducing manufacturing costs, ease of handling the system and robustness to thermal shock or thermal cycle [1,2]. We have been developing anode-supported SOFCs and have attained high conversion efficiency of 53% HHV [3,4] at 1023 K using the Cr-containing alloy interconnects. However, long-term stack tests revealed that the use of Cr-containing alloy interconnects degraded the performance of SOFCs [5], although an excellent stability of single-cells without alloy separators was confirmed [6]. Therefore, alloy separators are considered to degrade the performance of SOFC [7,8]. Some reports [9,10] have shown the deposited Cr at the interface between electrolyte and cathode decreased the cathode performance in half-cell tests. In this paper, we focused on the relationship between the oxide layer formed on several alloys and the degree of Cr-poisoning.

2. Experimental

2.1. Preliminary evaluation of the oxide scale formed on alloy surface

Three kinds of Cr-containing alloy materials, SUS430 (Nisshin Steel Co. Ltd., Japan), ZMG232 (Hitachi Metals Co. Ltd., Japan) and Inconel600 (Mitsubishi Material Co. Ltd., Japan), were annealed at 1073 and 1273 K in air for 2 h to investigate the oxide layer formed on the alloy surface. Surfaces of the annealed alloys were analyzed by X-ray diffractometry (XRD, BRUKER AXS Inc. M21X). The chemical compositions of the alloy materials are listed in Table 1.

2.2. Half-cell tests

The degree of Cr-poisoning was investigated for each alloy using a half-cell measurement method. A schematic illustration of the method is shown in Fig. 1. We used cylindrical pellets of electrolyte of 2 cm in diameter and 2 mm in thickness. For the reference electrode, a platinum paste of 0.3 mm in size was printed at the perimeter of the pel-

* Corresponding author.
E-mail address: k-fujita@tokyo-gas.co.jp (K. Fujita).

0378-7753/$ – see front matter © 2004 Elsevier B.V. All rights reserved.
doi:10.1016/j.jpowsour.2003.12.050

Table 1
Chemical compositions of the chromium-containing alloys used in this study

	Chemical composition (wt.%) of the chromium-containing alloy											
	Cr	Fe	Ni	Mn	Si	C	P	S	Al	La	Zr	Cu
SUS430 Nisshin Steel Co. Ltd.	16.03	82.27	0.29	0.91	0.42	0.06	0.018	0.001	–	–	–	–
ZMG232 Hitachi Metals Co. Ltd.	22.00	76.48	0.26	0.48	0.36	0.02	–	–	0.14	0.04	0.22	–
Inconnel600 Mitsubishi Material Co. Ltd.	14.00	6.00	77.80	1.00	0.50	0.20	–	–	–	–	–	0.5

let. For the cathode, $La_{0.6}Sr_{0.4}MnO_3$ (LSM), which was reported to easily lose activity by Cr-poisoning [11], was screen-printed on the center of the electrolyte surface, and sintered at 1423 K for 2 h. For the counter electrode, a platinum paste was screen-printed on the other side of cathode, and sintered at 1273 K for 10 h. Pt-mesh was set between the cathode and the alloy separator. The flow-rate of air was set 2 l/min, in order to supply sufficient dry air into the half-cell. An overvoltage and ohmic resistance were measured under a current density of 0.3 A/cm^2 at 1073 K.

At first, a half-cell test was performed using $La_{0.6}Sr_{0.3}CrO_3$ (LSC) ceramic as a separator, which was reported to be innocuous for the cathode. After that, three kinds of alloy materials were used as separator. The interface between the cathode and the electrolyte was examined by electron probe micro analyzer (EPMA, Shimadzu Co. Ltd., EPMA-870) after the tests. The surface and cross-section of the alloy were analyzed by scanning electron microscope and energy dispersion X-ray analysis (SEM/EDX, JEOL Ltd., EX-23000BU).

2.3. Single-cell stack tests

The degradation of single-cell stack performances was examined using ZMG232 and SUS430 separators. A schematic illustration of the measurement method for a cell stack module is shown in Fig. 2. The cell was manufactured by co-sintering of electrolyte–anode bilayer at 1773 K, followed by firing an interlayer of $Ce_{0.8}Sm_{0.2}O_{2-\delta}$ and a composite of $La_{0.6}Sr_{0.4}Co_{0.2}Fe_{0.8}O_3$/SDC cathode.

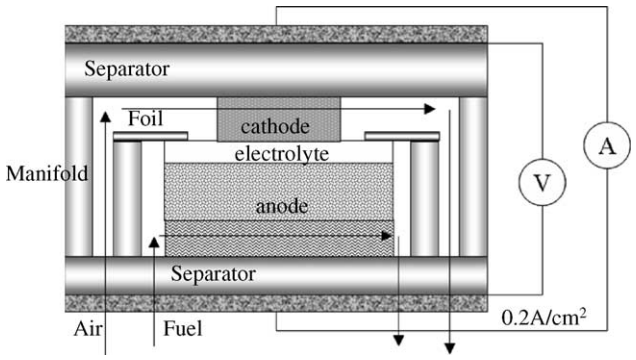

Fig. 2. Schematic illustration of measurement method for a single-cell stack module.

The single-cell was an anode-supported type having a thin electrolyte for reduced-temperature operation. The details of preparation process were written in a previous report [12]. The stack operation was conducted at a current density of 0.2 A/cm^2 at 1023 K using dry hydrogen and air.

3. Results and discussion

3.1. Preliminary evaluation of the oxide scale formed on the alloy surface

Cr-containing alloys were annealed at high temperatures formed various oxide layers on the surface. The Cr-containing alloy materials used in this study were a

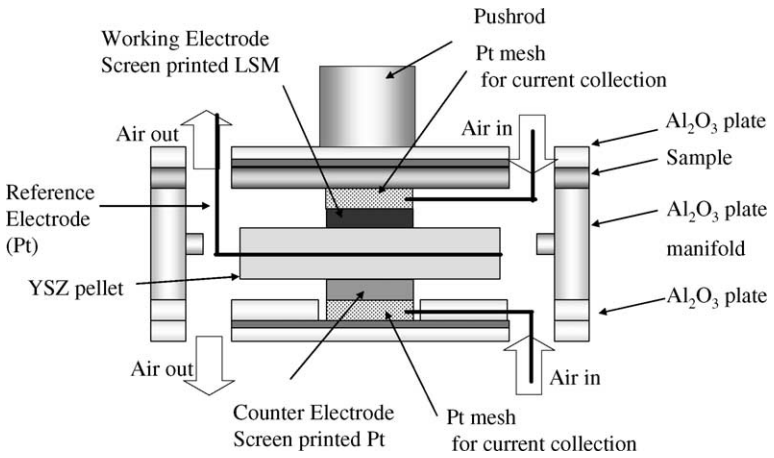

Fig. 1. Schematic illustration of measurement method for Cr-poisoning using a half-cell.

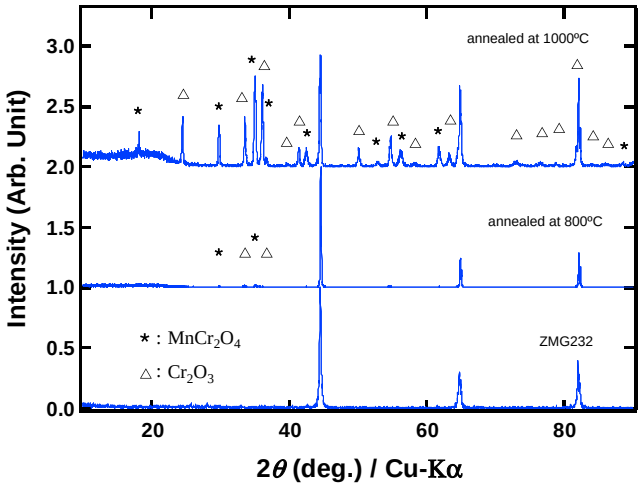

Fig. 3. XRD patterns for ZMG232 alloy surface.

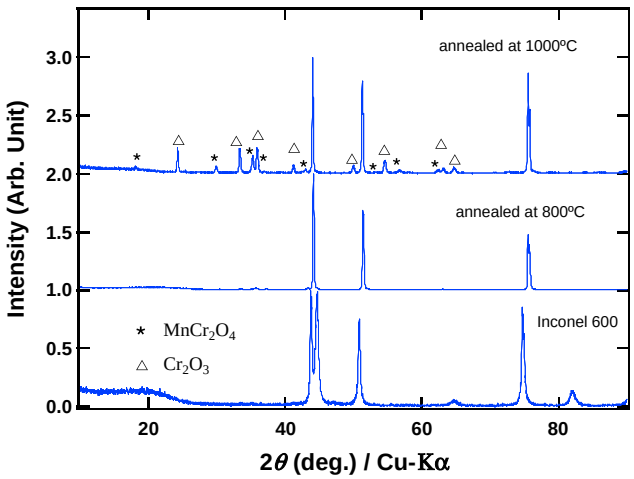

Fig. 5. XRD patterns for Inconel600 alloy surface.

nickel-based alloy (Inconel600) and ferrite system stainless steels (SUS430 and ZMG232). The difference in chemical compositions of SUS430 and ZMG232 can be characterized mainly by the quantity of Cr and Mn and the presence of Al and Zr. Generally, if aluminum is contained about 2% or more in the alloy, Al_2O_3 oxide layer will be formed on the surface at high temperatures, and the alloy will have high oxidation resistance. Even if the Al content is low in the alloy, Al diffuses toward the surface and maybe finally forms an Al_2O_3 layer. Therefore, the Al-containing alloy is considered to be not good for the separator since an electric conduction pass will be intercepted by the Al_2O_3 layer. The Al_2O_3 layer, however, was not formed in a short term test on ZMG232 in which Al content is 0.14%. The XRD patterns of the oxide layer formed on the Cr-containing alloy materials are shown in Figs. 3–5. Cr_2O_3 and $MnCr_2O_4$ were detected on ZMG232 surface after annealing at 1073 K, and the intensity was stronger at 1273 K. Other oxides, such as Al_2O_3 and SiO_2, were not detected. Cr_2O_3 and $MnCr_2O_4$ were also detected on the surface of SUS430 and Inconel600 annealed at 1273 K. Since the peaks of these oxides of SUS430 were sharp even at 1073 K, the oxide layer on SUS430 was considered to be generated easily as compared with that on ZMG232 and Inconel600. These results do not conflict with the reports [13,14] that ZMG232 and Inconel600 have high temperature resistance. These results indicate that the oxide layer of $MnCr_2O_4$ and Cr_2O_3 were formed on the alloy materials, and these oxides would affect the performance of a cathode in a half-cell test and a single-cell stack operation.

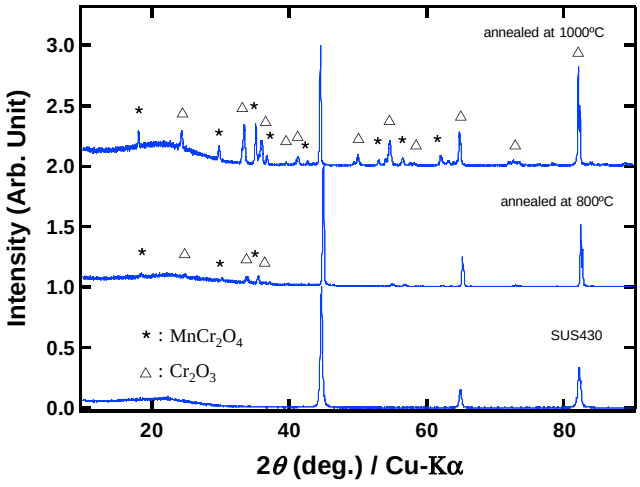

Fig. 4. XRD patterns for SUS430 alloy surface.

3.2. Half-cell test

Half-cell tests were performed for measuring the degradation of the cathode by Cr-poisoning. The results are shown in Fig. 6. At first, the half-cell test was carried out using a LSC ceramic separator. The absolute value of overvoltage (|OV|) decreased gradually with operation time. The decrease seems to be due to a “current effect”. This effect is considered to be caused by a change in the microstructure of the electrode [15], but the details for the mechanism have not been clarified. Since the LSC ceramic is chemically stable, the cathode did not degrade by vapor species from the LSC. In the case of the ZMG232 alloy separator, the |OV| increased rapidly in the initial stage at 7 h. The increase of the cathode polarization was considered to be caused by the Cr-poisoning. However, the |OV| of ZMG232 had a tendency to decrease at around 30 h of the operation time. The |OV| of Inconel600 and SUS430 increased with operation time over 100 h, and did not decrease. In order to examine the influence of Ni and/or Al in the alloy on the cathode degradation, the half-cell tests were carried out using Ni and 16Cr–3.3Al alloy as the separators. As a result, the electrochemical activity of the cathode was not affected by the elements. Based on these results, it can be concluded that the decrease of |OV| is related to the Cr_2O_3 formation on the alloy surface.

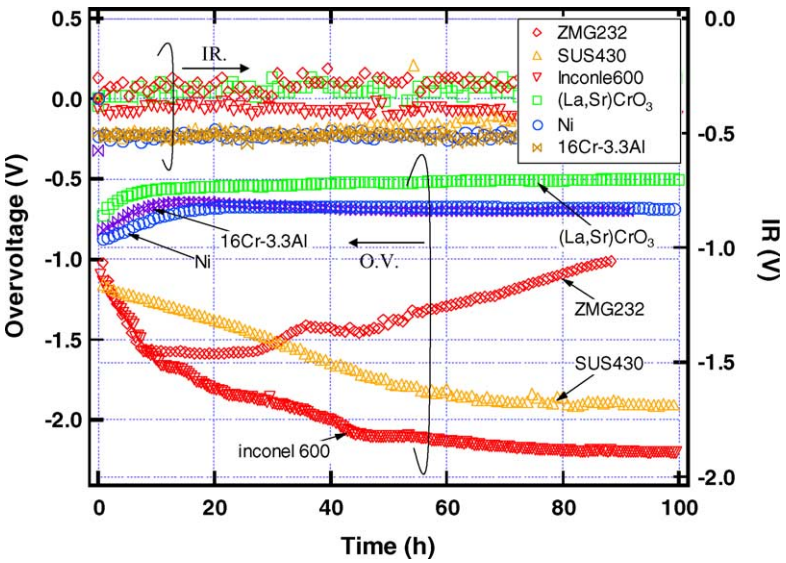

Fig. 6. The dependencies of overvoltage of half-cell test.

3.3. Cathode/electrolyte interface after the half-cell tests

Cross-sectional SEM/EPMA images of cathode/electrolyte interface after the half-cell tests using LSC, SUS430, Inconel600, and ZMG232 are shown in Figs. 7 and 8. The deposition of Cr was observed at the interface in the case of Cr-containing alloy separators, while Cr deposition was not detected with the LSC ceramic separator. The deposition of Cr at the interface should cause the increase of |OV| in the half-cell test, which is considered in previous reports [9–11]. In conclusion, the main element in the alloy which caused the degradation is chromium.

3.4. Oxide layer on the alloy surface after the half-cell test

Cross-sectional SEM/EDX images of the oxide layer formed on ZMG232 surface after a polarization for 23 and 90 h are shown in Fig. 9(a) and (b), respectively. Table 2 shows the quantitative analyses results of the alloy surface measured by EDX. The results show that $MnCr_2O_4$ layer was formed on the ZMG232 alloy surface, and Al_2O_3 precipitated in the ZMG232 alloy at around 20 μm from the surface. The $MnCr_2O_4$ layer and Al inner oxides increased with the polarization time. In the case of the ZMG232 alloy separator, |OV| showed relatively high resistance against

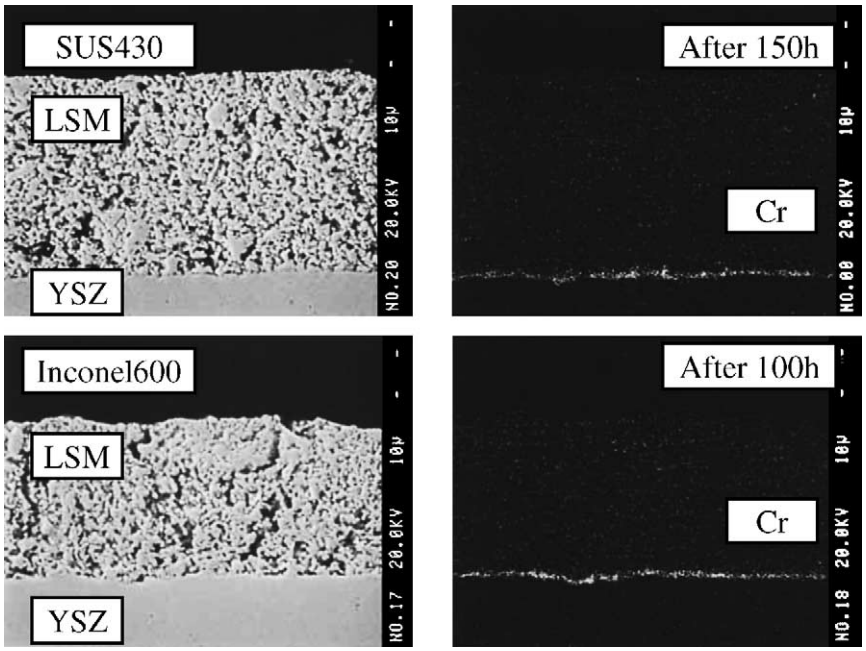

Fig. 7. SEM/EPMA images of the interface between YSZ electrolyte and LSM cathode using SUS430 and Inconel600 alloy after half-cell tests.

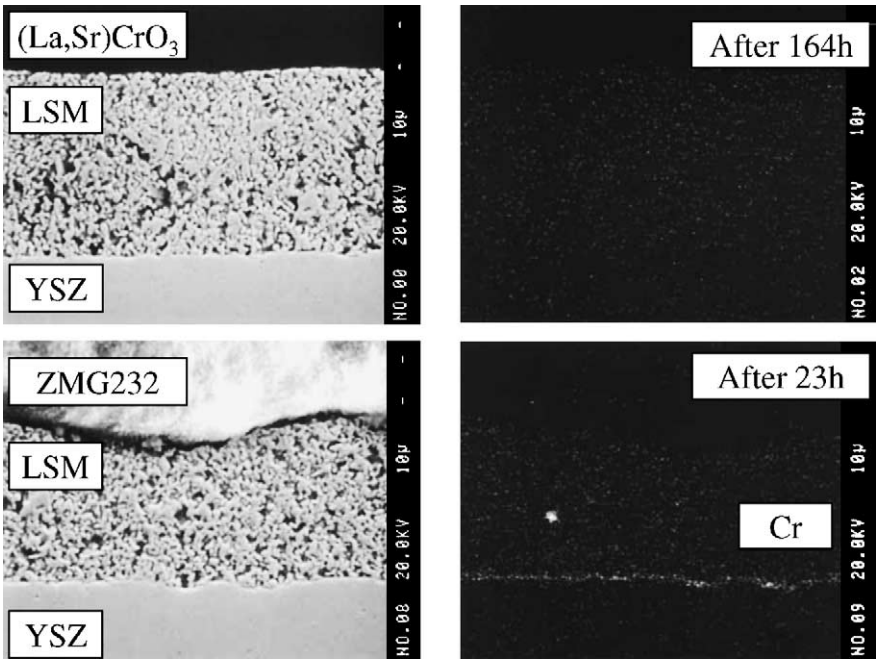

Fig. 8. SEM/EPMA images of the interface between YSZ electrolyte and LSM cathode using (La,Sr)CrO_3 ceramics and ZMG232 alloy after 24 h in half-cell tests.

Cr-poisoning. These results suggested that Cr-poisoning is reduced by the oxide layer of $MnCr_2O_4$ or Al_2O_3. Figs. 10 and 11 show the cross-sectional EDX images of Inconel600 and SUS430, and Table 2 shows the quantitative analyses results. The oxide layer of Mn could hardly be observed in Inconel600, while the oxide layer containing Cr and Mn are observed in SUS430. These results agree with the XRD patterns as shown in Fig. 5. The $MnCr_2O_4$ layer formed on SUS430 would be thicker than that on ZMG232 from XRD results, and |OV| with SUS430 was smaller than ZMG232 before 30 h. These results suggest that the $MnCr_2O_4$ layer is effective to reduce Cr-poisoning in the initial stage.

Next, we will discuss the turn to a decrease in |OV| using a ZMG232 separator at around 40 h after polarization. From Table 2, one can see that the amounts of Cr and Mn on the ZMG232 surface layer after 90 h and that of on the SUS430 after 150 h are almost comparable. This suggests that the formation of $MnCr_2O_4$ layer is not enough to prevent Cr-poisoning completely. Figs. 9(b) and 10 show that the Al inner oxide is peculiar to ZMG232. The |OV| of the cathode with the 16Cr–3.3Al separator, which formed the Al_2O_3 oxide layer, showed a constant value as shown in Fig. 6. It could be concluded that the recovery of |OV| of the cathode with ZMG232 separator resulted from Al contained in ZMG232.

Table 3
Chemical compositions of LSCF cathode surface in contact with ZMG232 alloy separator after a single-cell stack test

Elements	Point A (mol.%)	Point B (mol.%)
Cr K	7.23	50.07
Fe K	36.56	0.62
Co K	8.63	–
Sr L	12.63	46.82
La L	34.95	2.5

The points are shown in Fig. 13.

3.5. Single-cell stack test

The results of single-cell stack tests using SUS430 and ZMG232 separators are shown in Fig. 12. The cell voltage using the ZMG232 separator decreased rapidly and recov-

Table 2
Chemical compositions of the various Cr-containing alloy surfaces after polarization

Cr-containing alloy sample	Time for half-cell testing (h)	Chemical composition (mol.%)					
		Mn	Cr	Fe	Si	Al	Ni
ZMG232	23	7.13	21.25	7.58	1.01	0.13	–
ZMG232	90	15.46	17.21	2.69	0.03	0.24	–
SUS430	150	14.22	20.07	3.71	0.11	–	–
Inconnel600	100	2.20	27.16	1.03	0.16	–	4.10

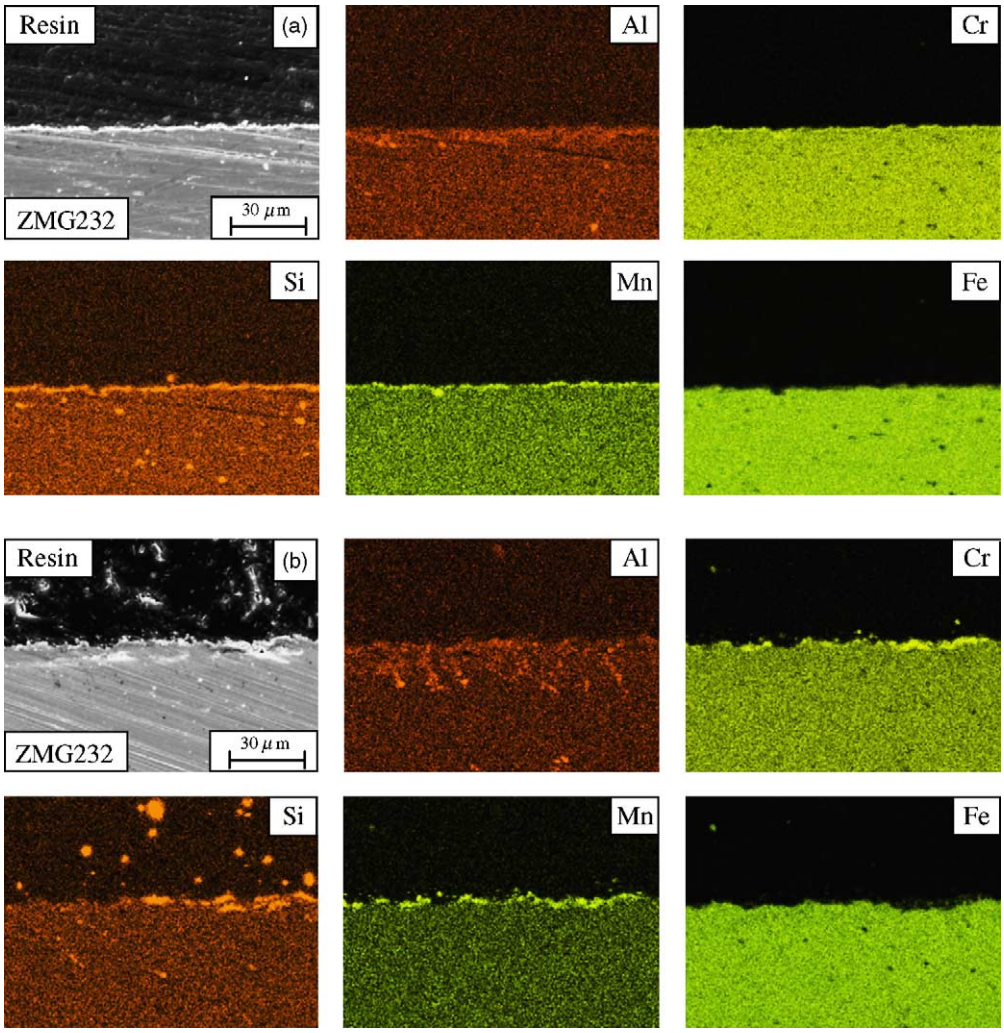

Fig. 9. (a) Cross-sectional SEM/EDX images of oxide layer formed on ZMG232 after a polarization for 23 h. (b) Cross-sectional SEM/EDX images of oxide layer formed on ZMG232 surface after a polarization for 90 h.

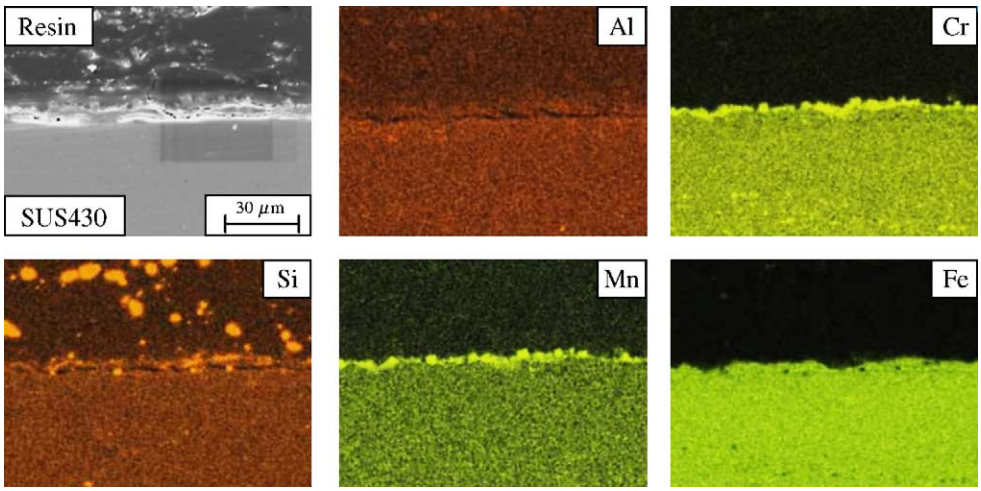

Fig. 10. Cross-sectional SEM/EDX images of oxide layer formed on SUS430 after a polarization for 120 h.

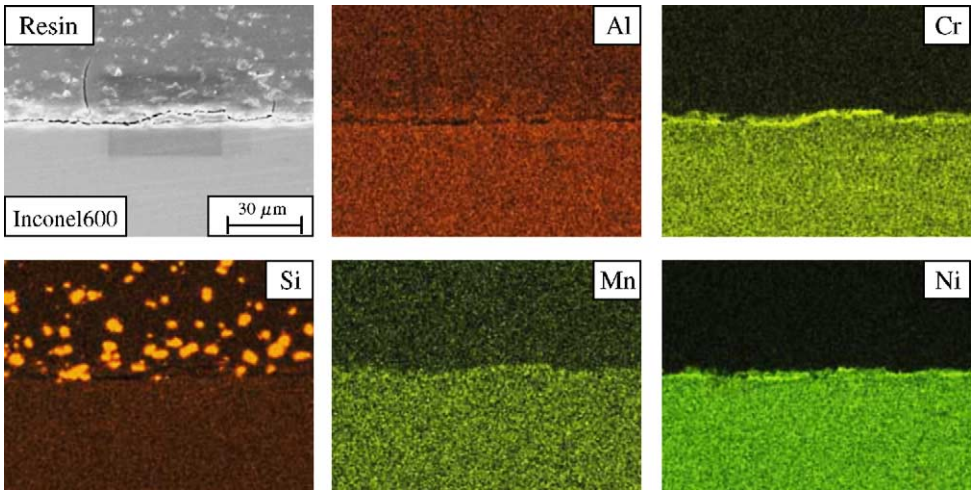

Fig. 11. Cross-sectional SEM/EDX images of oxide layer formed on Inconel600 after a polarization for 120 h.

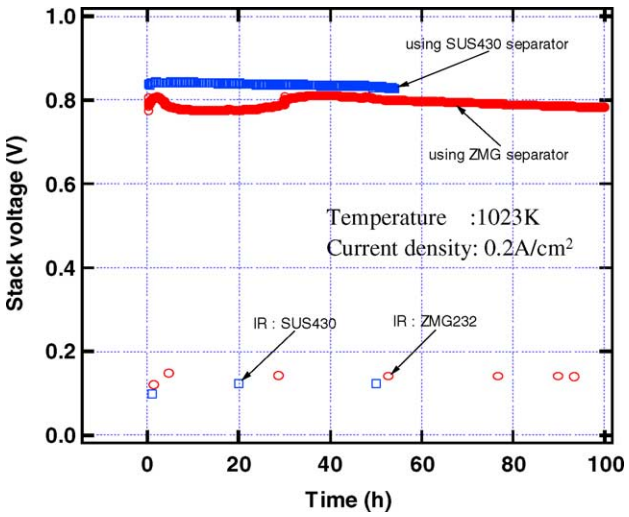

Fig. 12. Time dependencies of the voltage of single-cell stacks using ZMG232 and SUS430 alloy separator operated at 0.2 A/cm^2.

ered after 30 h similarly to the half-cell test. The stack voltage using SUS430 decreased with the operating time, which was similar to the half-cell test. These results indicate that the main degradation of the stack occurred in the cathode, and the half-cell test was proved to be useful to study the degradation of the cell stack. However, the terminal output voltage of the single-cell stack using ZMG232 decreased slightly even after 40 h, although the |OV| was recovering. The reason would lie in the direct contact of the alloy and the cathode in the stack. The EDX images of the cathode surface contacted with the ZMG232 are shown in Fig. 13, and the quantitative analysis results are shown in Table 3. Oxides of Sr and Cr covered the cathode surface partially. The ratio of Sr to Cr in the oxide was almost unity. In order to investigate the oxide, mixed powder of cathode and Cr_2O_3 were sintered at 1173 K for 50 h in air. The XRD pattern was measured and shown in Fig. 14. Formation of $SrCrO_4$ was detected, which indicates that the contact of

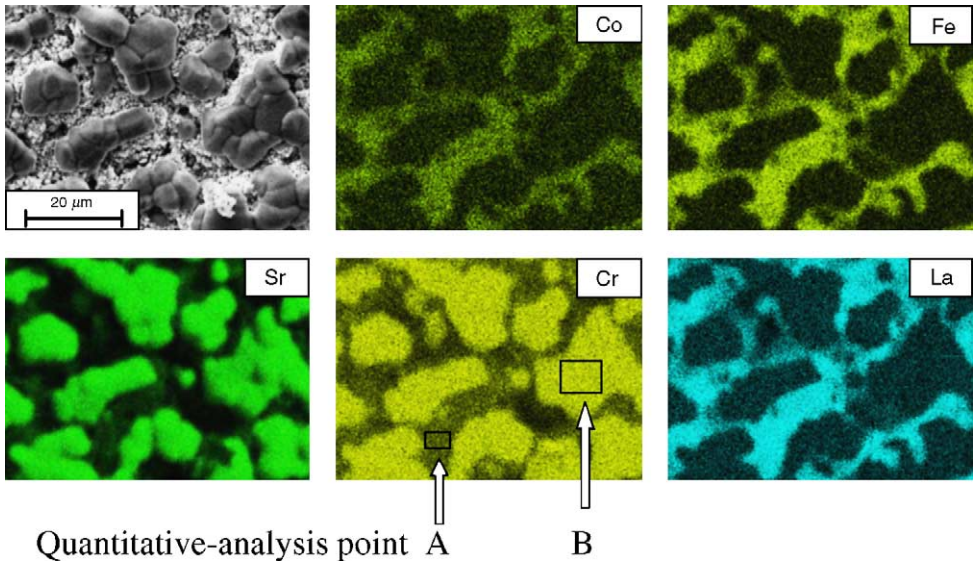

Fig. 13. SEM/EDX images of LSCF surface in contact with ZMG232 alloy.

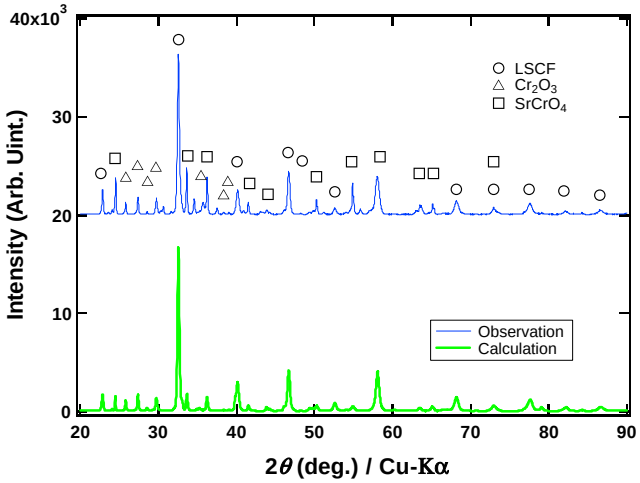

Fig. 14. XRD patterns of LSCF and Cr_2O_3 composite oxide.

the Cr-containing alloy with cathode promotes the formation of hexavalent Cr compounds. In order to prevent cathode degradation, it is important to avoid the direct contact of the alloy with the cathode when using Cr-containing alloy as separators.

4. Conclusion

We have investigated the relationship between the electrochemical properties of SOFC cathode and the composition of the oxide layer formed on the alloy separators. The main results are as follows:

1. $MnCr_2O_4$ grown on the ZMG232 and SUS430 surfaces, and is effective to reduce the Cr-poisoning in the initial stages.
2. The degradation using a ZMG232 separator was smaller than that of Inconel600 because of the effect of Al_2O_3 and $MnCr_2O_4$.
3. The contact with Cr-containing alloy and the cathode promoted the hexavalent Cr of $SrCrO_4$.

Acknowledgements

Part of this work was performed as R&D program of New Energy and Development Organization (NEDO). We would like to thank NEDO and Ministry of Economy, Trade and Industry (METI) for their advice and financial support.

References

[1] K. Huanig, P.Y. Hou, J.B. Goodenough, Characterization of iron-based alloy interconnects for reduced temperature solid oxide fuel cells, Solid State Ionics 129 (2000) 237.
[2] T. Brylewski, M. Nanko, T. Maruyama, K. Przybylski, Application of Fe–16Cr ferrite alloy to interconnector for a solid oxide fuel cell, Solid State Ionics 143 (2001) 131.
[3] Y. Baba, T. Ogiwara, H. Yakabe, Y. Matsuzaki, T. Sakurai, J. Electrochem. Soc., submitted for publication.
[4] Y. Matsuzaki, Y. Baba, T. Ogiwara, H. Yakabe, in: Proceedings of the Fifth European SOFC Forum, Lucerne, July 2002, p. 776.
[5] J. Pirón-Abellán, F. Tietz, V. Shemet, A. Gil, T. Ladwein, L. Singheiser, W. Quadakkers, in: Proceedings of the Fifth European SOFC Forum, Lucerne, July 2002, p. 248.
[6] Y. Baba, T. Ogiwara, H. Yakabe, Y. Matsuzaki, FC Seminar, Palm Springs, November 2002, p. 340.
[7] W. Köck, H. Martinz, H. Greiner, M. Janousek, in: S.C. Singhal, M. Dokiya (Eds.), Solid Oxide Fuel Cell IV, PV95-1, The Electrochemical Society Inc., 1995, p. 841.
[8] H. Greiner, T. Grögler, W. Köck, R.R. Singer, in: S.C. Singhal, M. Dokiya (Eds.), Solid Oxide Fuel Cell IV, PV95-1, The Electrochemical Society Inc., 1995, p. 879.
[9] Y. Matsuzaki, I. Yasuda, Solid State Ionics 126 (1999) 307.
[10] Y. Matsuzaki, I. Yasuda, J. Electrochem. Soc. 148 (2001) 126.
[11] Y. Matsuzaki, I. Yasuda, Solid State Ionics 132 (2000) 271.
[12] Y. Matsuzaki, I. Yasuda, Solid State Ionics 152 (2002) 463.
[13] T. Horita, Y. Xiong, K. Yamaji, N. Sakai, H. Yokokawa, in: Proceedings of the Fifth European SOFC Forum, Lucerne, July 2002, p. 401.
[14] T. Horita, Y. Xiong, K. Yamaji, N. Sakai, H. Yokokawa, J. Power Sources 118 (2003) 35.
[15] H. Tsukuda, A. Yamashita, K. Hasezaki, J. Ceram. Soc. Jpn. 105 (1997) 862.